


RESEARCH ARTICLE OPEN ACCESS

Pixelated Laser with Tailored Emission Spectrum Photopatterned by Digital Holographic Microscopy

 Sudharsana Bhashyam Pillailokam | Alex Berdin | Arri Priimagi 

Smart Photonic Materials, Faculty of Engineering and Natural Sciences, Tampere University, Tampere, Finland

Correspondence: Arri Priimagi (arri.priimagi@tuni.fi)

Received: 11 February 2026 | **Revised:** 30 March 2026 | **Accepted:** 3 April 2026

Keywords: azobenzene | digital holographic microscope | holography | organic DFB lasers | pixelated laser | surface relief gratings

ABSTRACT

Organic thin-film distributed feedback lasers provide broad spectral tunability and structural flexibility. However, the realization of spatially programmable multiwavelength emission across a 2D device area remains a challenge. In this study, this challenge is addressed through programmable fabrication of microresonator geometries using a system that integrates digital holographic microscopy with holographic lithography. Microresonators are first inscribed on an azobenzene-containing thin film as surface-relief gratings over localized regions known as pixels via holographic lithography. The pixelated pattern is then transferred onto the active medium using a soft-lithographic direct-transfer method to form the lasing structure. This approach enables controlled variation of the microresonator geometry, allowing precise tailoring of the laser emission spectrum. We demonstrate both single-wavelength emission from individual pixels and simultaneous multiwavelength lasing from collectively excited pixel arrays. The presented strategy provides a scalable platform for programmable organic laser arrays with arbitrary 2D spectral layouts.

1 | Introduction

Organic thin-film distributed feedback (DFB) lasers represent a versatile class of coherent light sources owing to their compact geometry, low-cost fabrication, and compatibility with solution-processable gain media [1–5]. In these devices, optical gain is provided by emissive organic materials such as laser dyes embedded in polymer hosts [6]. Optical feedback is provided by periodic modulation of the refractive index, typically implemented as a diffraction grating within or on top of the active layer [7–9]. The inherent dependence of emission wavelength on the gain medium and resonator parameters has enabled a wide range of strategies for spectral control in organic DFB lasers. Such spectral control has been achieved by variation of the effective refractive index via thickness gradients [10], mechanical deformation of elastomeric substrates [11, 12], or by employing different gain media with distinct emission characteristics [13]. Wavelength

selection has also been realized by fabricating gratings with different periodicities through multi-step lithographic processes or controlled fabrication conditions [14].

As the demand for compact, multifunctional photonic devices has increased, particularly in applications such as multiplexed biosensing [15, 16], spectrally encoded imaging [17, 18], and planar lightwave circuits [19], there has been a growing interest in realizing multi-wavelength emission from a single device platform. One approach to achieve this involves structuring multiple gratings with distinct periods in spatially separated regions of the device, thereby creating localized emission zones [20–25]. These spatially defined regions are often interpreted as pixels, where each region supports lasing at a specific wavelength determined by its local grating period. Such implementations have been enabled through a variety of fabrication strategies, including E-beam lithography, nanoprinting, and ink-jet printing.

This is an open access article under the terms of the [Creative Commons Attribution](https://creativecommons.org/licenses/by/4.0/) License, which permits use, distribution and reproduction in any medium, provided the original work is properly cited.

© 2026 The Author(s). *Advanced Optical Materials* published by Wiley-VCH GmbH

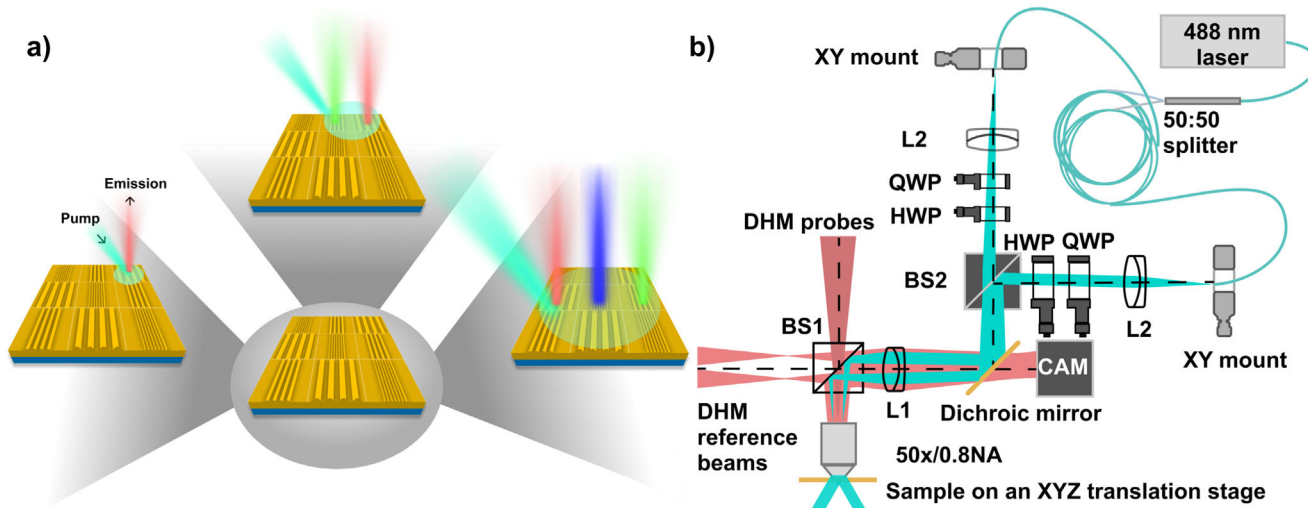


FIGURE 1 | (a) Scheme of a pixelated laser design illustrating facile emission control through selective excitation of pixels by adjusting the pump spot size and location. (b) Scheme of the DHM-integrated holographic lithography setup used for the inscription of pixelated surface relief gratings.

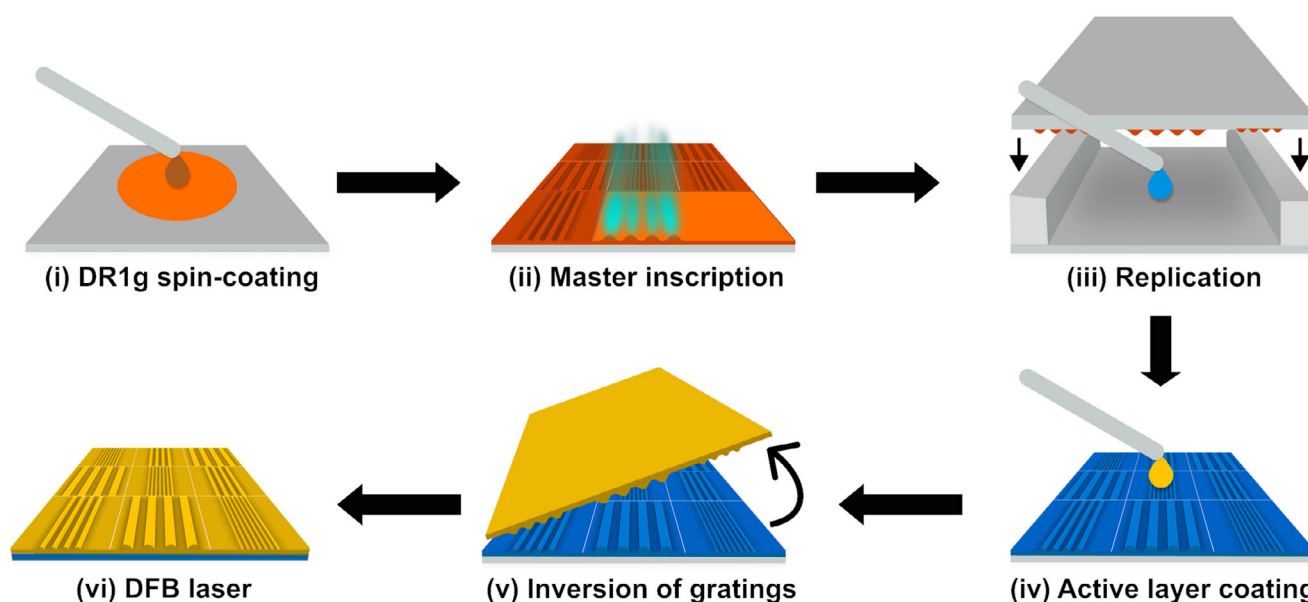


FIGURE 2 | Schematic of the pixelated laser fabrication process: (i) DR1g is spin-coated on a glass substrate. (ii) Pixelated SRGs are inscribed as master gratings on DR1g film by holographic lithography. (iii) The gratings are replicated onto PDMS in a replication cell and subsequently cured thermally. (iv) An organic gain medium is coated onto the PDMS replica to form the active layer with DFB resonator. (v) The resulting thin-film laser membrane is inverted by direct-contact transfer to (vi) establish the required refractive index contrast for lasing.

Despite advances in pixelated organic DFB lasers, current methods for creating multi-wavelength emission patterns remain constrained by limited automation and programmability. Existing approaches typically rely on sequential fabrication steps or predefined templates, which restrict the complexity and independent control of grating parameters across a 2D device area. Although post-fabrication tuning of emission via pump laser position and spot size has been demonstrated [26, 27], such approaches operate only on pre-existing gratings and provide limited flexibility in defining complex 2D pixel patterns. As a result, there remains a need for fabrication strategies that enable automated, spatially resolved, and independently programmable grating inscription,

while still allowing complementary post-fabrication spectral adjustments for enhanced device versatility.

The emergence of surface-relief gratings (SRGs) in azobenzene-containing polymer (azopolymer) films, photoinduced by holographic lithography [28, 29], has provided a simpler and more scalable route for fabricating diffraction gratings. SRGs are periodic sinusoidal surface corrugations formed through mass migration under interference illumination of azopolymer films. During this process, the light interference pattern is recorded onto the polymer thin film in the form of an SRG with controlled period and modulation depth, mediated by the photochemical

isomerization of azobenzene moieties [30]. Owing to the one-step, maskless fabrication and high structural fidelity, holographic SRG inscription has been widely adopted for implementing DFB resonators in organic thin-film lasers, enabling narrow linewidth, low threshold, and wavelength-selective emission [31–35]. In addition, recent developments in holographic lithography and photoresponsive polymers have enabled the inscription of complex [36–38] and spatially localized [39] SRG structures. However, their integration into functional laser architectures, particularly with reliable transfer onto active thin-film gain media, remains largely unexplored.

In this work, we address this gap by introducing a fully automated fabrication strategy for spatially discretized DFB microresonators, or pixels, with independently defined grating periods. Localized SRGs are inscribed onto azobenzene-containing films using a customized holographic lithography setup combined with digital holographic microscopy (DHM). In this approach, 2D pixel arrangements with independently defined grating parameters are directly specified and inscribed in a single step with high spatial fidelity [40]. The pixelated grating array is then transferred onto the active gain medium through a soft-lithographic direct-transfer process, preserving the integrity of the grating profile. This approach allows precise spatial assignment of emission wavelengths across the device (Figure 1a), supporting both individually addressable single-wavelength lasing and simultaneous multi-wavelength emission from pixel arrays. Furthermore, emission wavelengths can be fine-tuned post-fabrication via pump laser location and spot size, providing an additional degree of spectral flexibility. By combining programmable pixel-level inscription with scalable transfer and optional post-fabrication tuning, this method establishes a versatile platform for high-throughput, programmable organic DFB lasers with arbitrary 2D spectral layouts.

2 | Results and Discussion

The fabrication of the organic thin-film DFB lasers involved the inscription of master gratings in the form of SRGs on azobenzene-containing thin films, followed by replication into a PDMS substrate and transfer of the gratings to the laser active layer membrane. The master gratings were inscribed on Disperse Red 1-containing molecular glass (DR1g), which exhibits rapid and efficient SRG formation under interference illumination in the blue-green region [41] and has been widely employed in our previous azobenzene-based SRG studies [34, 35, 39, 40, 42, 43]. Integration of the photolithography setup with a DHM (Figure 1b) enabled localized, pixel-by-pixel exposure of the DR1g films [40]. An aperture was used to expose a square pixel of $80 \times 80 \mu\text{m}^2$ to form a single microfabricated grating unit on the DR1g surface. Sequential exposure of these pixels produced an array of SRGs, each forming a distinct microresonator geometry. For vertical emission, the grating period Λ was designed according to the second-order ($m = 2$) Bragg condition (Equation (1)), which relates Λ to the desired emission wavelength λ_{las} .

$$m\lambda_{\text{las}} = 2n_{\text{eff}}\Lambda \quad (1)$$

The effective refractive index of the fundamental guided mode was numerically calculated to be $n_{\text{eff}} = 1.45$ using a slab wave-

guide model, neglecting the perturbation induced by the gratings. By tuning the grating period of different microresonators, the emission wavelength could be selectively adjusted within the spectral range supported by the gain medium. Multiple master gratings with varying microresonator arrangements were fabricated in this manner and subsequently replicated onto a polydimethylsiloxane (PDMS, $n = 1.412$) surface using assembly-cell process, as illustrated in Figure 2. Following replication, the organic gain layer was formed by spin-coating a solution of dye-doped polymer matrix in methyl ethyl ketone (MEK) on the PDMS replica. Polyvinyl acetate (PVAc, $n = 1.4665$) and DCM2 (4 wt% concentration in PVAc) were chosen as the polymer matrix and organic dye, respectively. Additionally, the polymer matrix was plasticized with 10 wt% of 2-(2-methoxyethoxy) ethanol (DEGME) to lower its Young's modulus. The active layer thickness was optimized by adjusting the spin-coating speed and concentration of the dye-polymer solution to achieve single-mode (fundamental) propagation with strong optical confinement.

During spin coating, the surface-relief pattern of the replica was imprinted onto the active film at their interface, forming a corresponding grating structure. To establish the refractive-index contrast required for low-threshold lasing, the grating pattern was subsequently inverted using direct-transfer process [34]. In this step, plasma-activated PDMS surface was brought into contact with the DFB membrane, allowing it to adhere and be lifted off while the original replica was separated. This inversion yielded a top-layer resonator configuration [22], which has been reported to provide stronger optical feedback and improved lasing efficiency in comparable systems [44]. Atomic force microscopy (AFM) images of the master gratings, replica, and final DFB membrane (Figure 3) show replication of the SRGs by retaining their sinusoidal shape and periodicity. The shallower gratings of the replica compared to the master gratings can be attributed to the incomplete capillary filling of PDMS due to trapped air bubbles within the submicron period gratings [45]. The minor imperfections observed in the transferred thin-film membrane are attributed to localized wrinkling arising from strain relaxation and mechanical deformation of the PDMS during the final transfer step. Optimizing the stiffness of the PDMS and ensuring uniform delamination can minimize such defects and enhance membrane uniformity.

The emission properties of the pixelated lasers were examined by fabricating and testing pixel patterns of appropriate periods. The grating periods were chosen according to emission wavelengths that could have a strong overlap with the gain spectrum of the active layer measured using the variable stripe length (VSL) method (shown in Figure 4a inset) [34]. As the maximum gain of the active layer is around 640 nm, three periods of 428, 435, and 442 nm were chosen with an anticipated emission around 620, 630, and 640 nm, respectively. The spectral selectivity, versatility, and tunability of the pixelated lasers were investigated with different pixel arrangements. Additionally, the pump spot diameter was also altered to change the pixel exposure to pump according to the requirements in the following experiments. Figure 4a shows the emission from a single pixel pumped with a spot size comparable to the pixel dimension in a laser with a 428 nm period. A single-mode emission at 623 nm demonstrates that even a single pixel with an appropriate period can function as a resonator providing sufficient optical feedback for lasing.

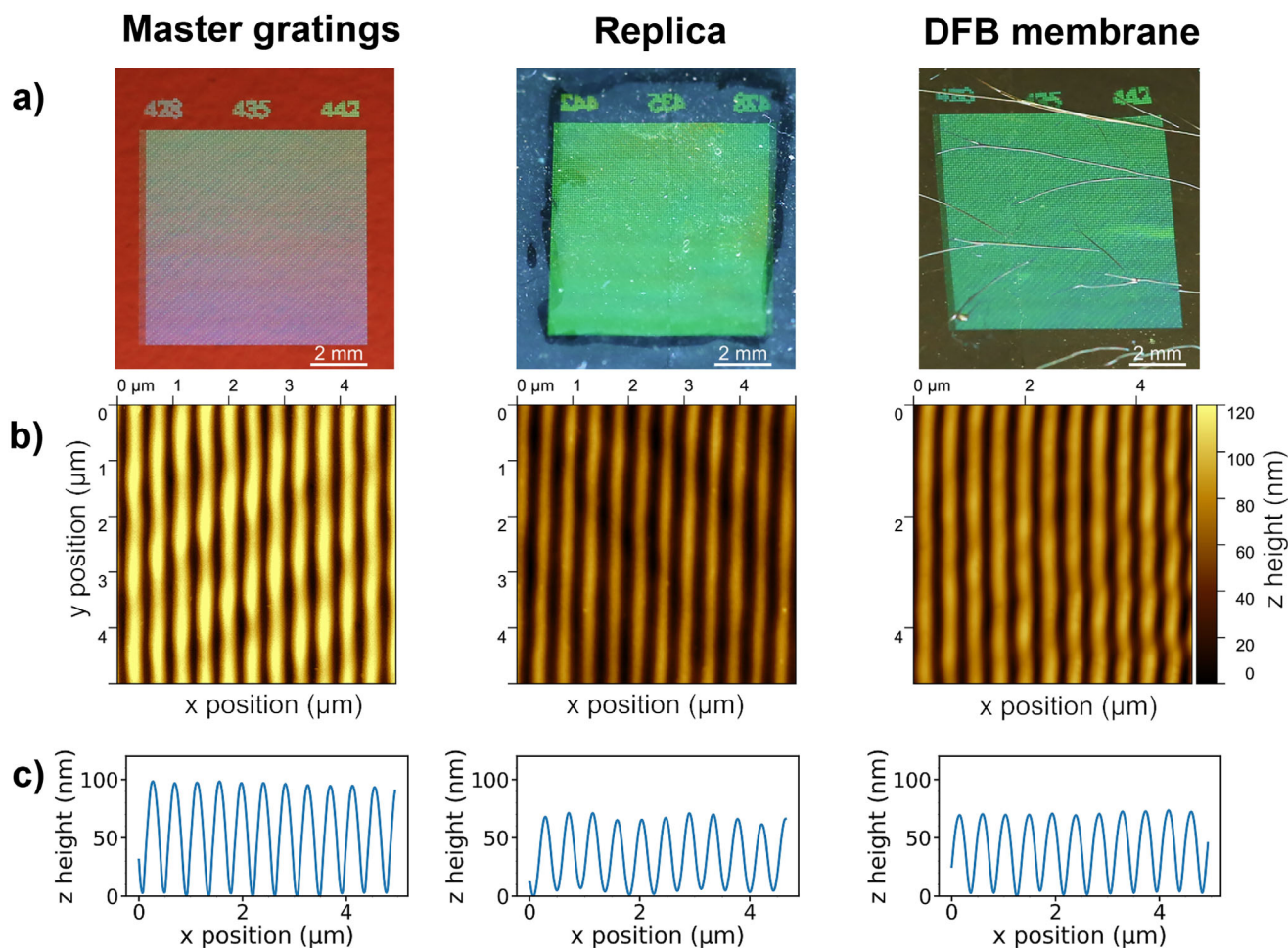


FIGURE 3 | (a) Photograph of master SRGs, PDMS replica and inverted DFB membrane laser. (b) 2D AFM image from one of the selected pixels from the corresponding sample. (c) Surface profile of the respective pixel.

The narrow lasing peak with a spectrometer resolution-limited linewidth (full width at half maximum, FWHM = 0.20 nm) is attributed to the TE_0 mode, characteristic of fundamental guided-mode operation in DFB polymer lasers [46, 47]. The active layer thickness was optimized to 1.8 μm to facilitate stable single-mode operation and reliable membrane transfer without mechanical deformation. Although this thickness lies above the cutoff for the TE_1 mode, its suppression is attributed to the lower threshold of the fundamental TE_0 mode. The ability of pixelated lasers to simultaneously emit multiple wavelengths was demonstrated by pumping a laser with an alternating pixel pattern containing two periods of 435 and 442 nm, as shown in the inset of Figure 4b. Collective pumping of these pixels led to simultaneous laser emissions around 630 and 640 nm corresponding to the two pixel periods, as shown in Figure 4b. An extension of this multiwavelength emission to a pixelated laser with three periods of 428, 435, and 442 nm exhibits a spectrum with an additional lasing peak, as depicted in Figure 4c. When such a DFB membrane was pumped, a minimum spot diameter covering three pixels was used to ensure collective excitation of all different periods. The CMOS image of the emission from a 3×3 pixel area is shown in the inset of Figure 4c. The above results demonstrate the concept of simultaneous multiwavelength laser emission using the pixelated laser approach. Finally, Figure 4d shows the emission from the same laser structure under serial excitation of individual pixels.

In contrast to the collective excitation described above, this configuration selectively activates the emission associated with individual pixel periods. The complementary behavior between collective and serial excitation highlights the flexibility of the present approach, where the combination of pixelated grating design and the organic gain medium enables controlled tailoring of the emission spectra within a single DFB membrane.

A slight shift of the lasing wavelength from desired emission wavelength given by Equation (1) was observed in most spectra. This behavior arises from the photonic stopband created by the DFB gratings, which is generally centered at the Bragg wavelength. Two Bloch modes form at the band edges whose separation depends on the grating depth and the modal overlap. Laser emission occurs at the edge mode that overlaps best with the gain peak and exhibits the lowest threshold [48]. In organic semiconductor DFBs, lasing typically appears closer to the long-wavelength edge of the stopband due to asymmetric losses [49]. The larger wavelength shifts of approximately 7–8 nm observed in some samples (e.g., Figure 4c) are attributed to uncertainties in the effective refractive index arising from the simplified waveguide model. In addition, small but sharp features that appear near the main lasing peaks are attributed to imperfections introduced during the final membrane-transfer step. Slight expansion or contraction of the DFB membrane on

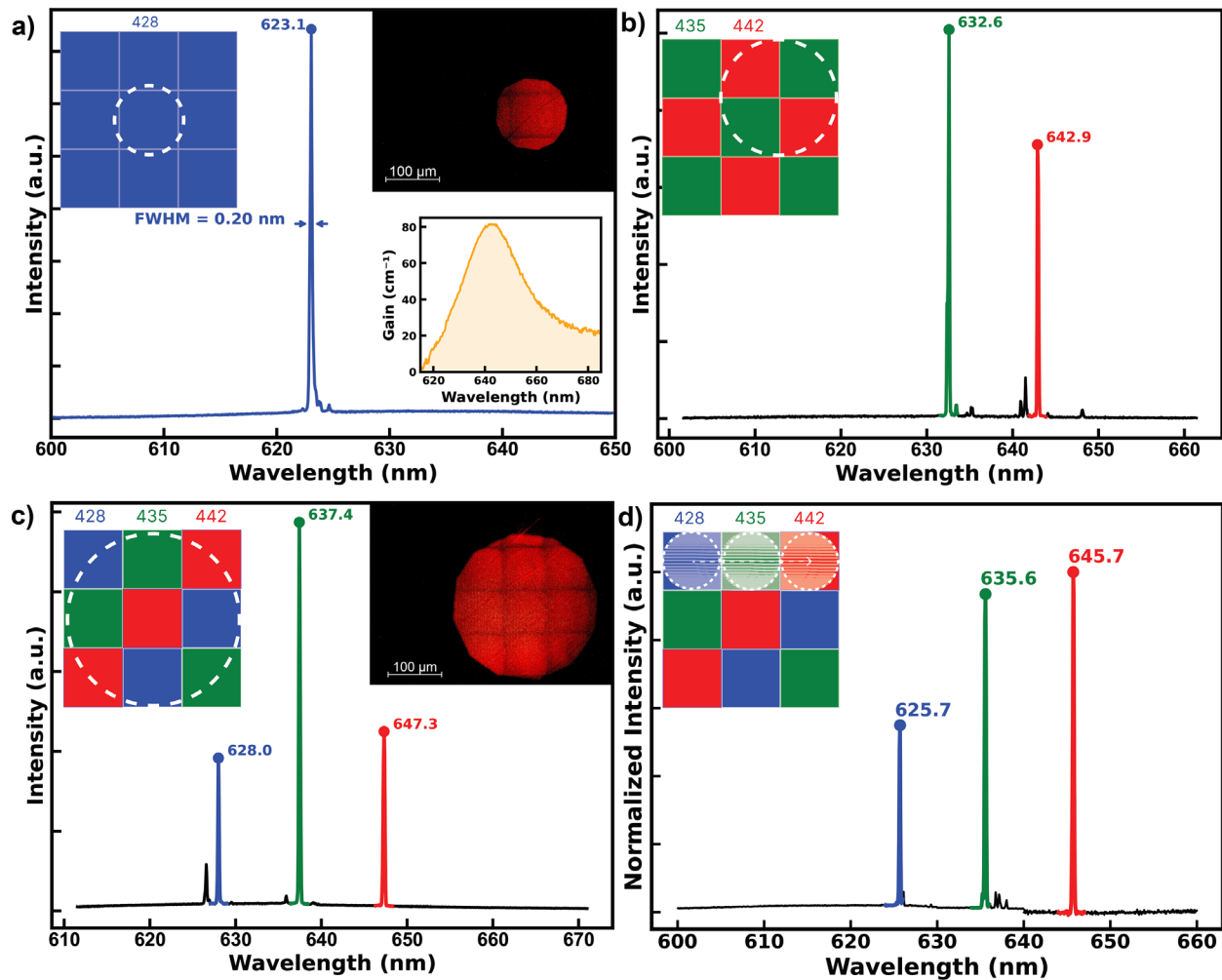


FIGURE 4 | (a) Emission spectrum of a single pixel laser with period of 428 nm. Lower right inset shows the gain spectrum of DCM2/PVAc. (b) Emission spectrum of a pixelated laser array with periods of 435 and 442 nm. (c) Emission spectrum of the pixelated laser array with periods of 428, 435, and 442 nm under collective excitation of all pixels. (d) Emission spectra of the pixelated laser array with periods of 428, 435, and 442 nm under sequential individual excitation. All the upper left insets show respective designs with the excited region and right insets show corresponding CMOS images of the emission from the pixelated laser.

the PDMS support can also locally modify the grating period in certain regions. Where the optical feedback remains sufficient in these regions, weak lasing emission can arise at wavelengths slightly displaced from the anticipated position, giving rise to low-intensity, spectrally shifted peaks.

The input-output characteristics of the pixelated lasers were investigated for the designs shown in Figure 4c by varying the pump power and measuring the output signal. The results exhibit a typical threshold behaviour of optically pumped lasers, where the emission intensity initially increases gradually with pump energy due to spontaneous emission. Beyond a characteristic threshold, the onset of stimulated emission and net optical gain overcoming cavity losses results in a sharp rise in output power, signifying the lasing transition. Figure 5a shows a representative threshold curve of a pixelated laser with a four-pixel resonator size, and the respective threshold energies of the lasers were determined to be 7.2, 5.1, and 6.5 μJ , corresponding to the excitation fluences of 2.8, 2.0, and 2.5 mJ cm^{-2} , respectively. These threshold energies and fluences exceed the reported threshold

(32 $\mu\text{J cm}^{-2}$) for DFB systems that employ the same gain medium and resonator structure by several orders of magnitude [34]. Such elevated thresholds can be attributed to the restricted resonator area available for feedback, which reduces mode confinement and effective gain [23]. This effect was systematically investigated by analyzing the input–output characteristics of pixelated laser arrays of varying resonator size from a single pixel ($80 \times 80 \mu\text{m}^2$) to twenty five pixels ($400 \times 400 \mu\text{m}^2$). To maintain experimental consistency, the number of simultaneously pumped resonators was kept constant by adjusting the diameter of the pump spot while keeping the intensity constant with an aperture.

Figure 5b summarizes the dependence of the threshold fluence on the size of the resonator in which a monotonic decrease in the threshold fluence can be observed with increasing resonator size. This trend arises because larger resonators provide greater gain volume and an extended feedback region, thereby reducing the net amplification required per unit length [2, 50]. In contrast, smaller resonators contain fewer grating periods, leading to

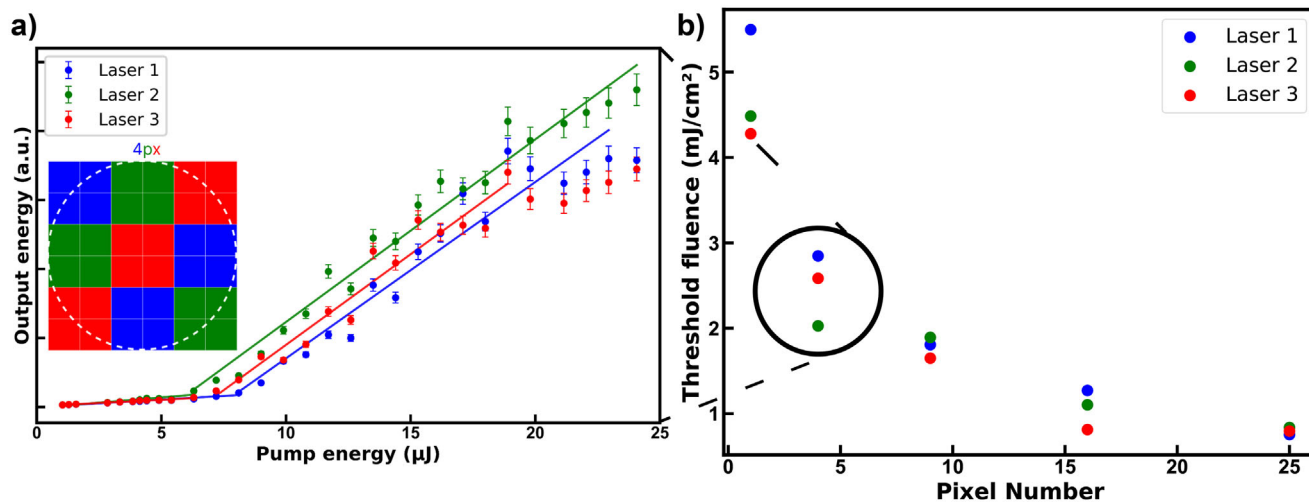


FIGURE 5 | (a) Input–output characteristics of the pixelated lasers with 4 pixel resonator size. Note the expansion of the collectively excited pump region shown in the inset. (b) Threshold fluence comparison of different resonator sizes.

weaker distributed feedback and increased relative losses, as boundary losses become more dominant for shorter cavities [14]. However, the decrease in threshold fluence is not linear for larger-area resonators consisting of multiple pixels stitched together. As the aperture opens to increase the diameter of the pump spot, the initially illuminated region coincides with the peak of the Gaussian pump profile. At larger spot sizes, the aperture exposes more of the lower-intensity areas of the Gaussian beam, leading to a less pronounced decrease in threshold fluence. Although the minimum measured threshold fluence remains higher than typical values reported for organic thin-film DFB lasers, these results are expected considering that even the largest resonator ($400 \times 400 \mu\text{m}^2$) is smaller than standard DFB cavity dimensions. The distinct fabrication method employed in this work together with additional losses associated with imperfect pixel stitching contribute to the elevated threshold fluences relative to conventional DFB systems.

These experiments demonstrate the flexibility of the pixelated laser approach for tailoring the emission characteristics through both maskless pre-fabrication design and post-fabrication optical excitation. The emission wavelengths are defined by the spatial arrangement of SRG periods during fabrication, while the number of simultaneously active lasing channels can be selected post-fabrication by adjusting the pump spot size. This dual-level control enables programmable multiwavelength emission within a single laser membrane. However, practical lower limits are imposed by fabrication resolution and pumping geometry. In particular, multiwavelength emission requires both multiple distinct SRG periods and a pump spot size commensurate with the corresponding resonator area; neither a single-period grating nor excitation confined to a single pixel can support simultaneous multiwavelength lasing. These constraints define the operational boundaries of emission programmability in the present system.

3 | Conclusion

This study demonstrates a DHM-integrated holographic lithography approach for the programmable fabrication of organic

thin-film pixelated DFB lasers with precisely tailored emission spectra. Microresonators inscribed as SRGs on azobenzene films and subsequently transferred onto the active medium enable single-wavelength emission from individual pixels and simultaneous multiwavelength lasing from collectively excited pixel arrays, as exemplified using grating periods of 428, 435, and 442 nm. The maskless nature of this approach enables direct assignment of grating parameters at the pixel level, overcoming the static constraints of conventional DFB fabrication. The ability to define independent grating periods across a 2D pixel array allows the realization of arbitrary spectral layouts, including randomized pixels for spectral encoding or non-linear arrays. In addition, emission characteristics can be further tuned via pump spot size and position, providing complementary post-fabrication control. The demonstrated operation of single-pixel resonators ($80 \times 80 \mu\text{m}^2$) highlights the potential for miniaturized and spatially addressable laser sources.

Beyond multiwavelength emission, the flexibility of the fabrication approach may be extended to more complex grating geometries, offering a potential route toward spatially structured emission and structured light generation with appropriate design. Overall, this work establishes a scalable platform for programmable organic DFB laser arrays with arbitrary 2D spectral distributions, with potential applications in sensing, integrated photonics, and emerging display technologies. Further optimization of lasing thresholds will be important for advancing practical implementations.

4 | Experimental Section

4.1 | Sample Preparation

A 5 wt.% solution of DR1g was initially prepared in a chloroform/1,2-dichloroethane mixture (80:20 vol.%) as the azobenzene-based inscription medium for the master gratings. The solution was filtered through a $0.2 \mu\text{m}$ polytetrafluoroethylene (PTFE) membrane filter and

subsequently spin-coated onto microscope-glass substrates at 3000 rpm for approximately 30 s. The resulting thin-film samples were dried at 65°C for 1 h. Surface-relief gratings (SRGs) with various periodicities were then inscribed on the DR1g films using a photolithographic setup integrated into a digital holographic microscope [40]. Following the inscription of the master gratings, a replication cell was assembled using a 500 μm spacer. A 10:1 mixture of polydimethylsiloxane (PDMS, Sylgard 184) base and curing agent was infiltrated into the empty cell by capillary action. After curing for 4 h at 65°C, the PDMS replica was peeled from the cell, yielding a high-fidelity replication of the master grating structures. For the active layer, a solution of poly(vinyl acetate) (PVAc, Sigma-Aldrich, MW = 500 000, $n = 1.4665$) in methyl ethyl ketone (MEK) (7.5 g/150 mL) was prepared. DCM2 (4-(Dicyanomethylene)-2-methyl-6-[2-(2,3,6,7-tetrahydro-1H,5H-benzo[*ij*]quinolizin-9-yl)vinyl]-4H-pyran) was added at a concentration of 4 wt.% relative to the polymer, and 10 wt.% 2-(2-methoxyethoxy) ethanol (DEGME) was included as a plasticizer. This dye-doped polymer solution was dynamically dispensed and spin-coated onto the PDMS replica at 5000 rpm to form the gain layer for lasing. To establish the refractive-index contrast required for optical confinement, the coated layer was subsequently transferred in an inverted orientation onto a flat PDMS film, leaving the gratings exposed to air. The surface profiles of the master grating, the PDMS replica, and the final DFB membrane were characterized using an atomic force microscope (AFM, Bruker icon) operated in ScanAsyst mode.

4.2 | Photolithographic Setup

SRGs were inscribed on DR1g thin films using a setup that integrates a digital holographic microscope (DHM R-2100, LyncéeTec) with a custom-built two-beam holographic lithography module [40]. A 488 nm single-mode diode-pumped laser (Coherent Genesis CX-488 2000) served as the inscription source. The laser output was divided into two beams of equal intensity using a fiber splitter, and their polarizations were adjusted using a combination of quarter-wave and half-wave plates. To maximize diffraction efficiency and modulation depth, the beams were set to right-circular polarization (RCP) and left-circular polarization (LCP) [51]. The interference field of these two beams with a uniform intensity of 18 W cm^{-2} , and periodically varying polarization distribution was focused onto the sample stage through a 50x, 0.8 N.A microscope objective to form the SRGs. In this configuration, the DHM served primarily as an interferometric projection platform in which the fiber-coupled beams were introduced through the DHM input ports and focused by the objective lens onto the sample plane. This arrangement enabled spatial confinement of the interference field to micrometer-scale regions, allowing sequential pixel-by-pixel SRG inscription through synchronized stage translation. The SRG periods were tuned as required by actuating the fiber-end positioning stages. The integrated DHM employed probe and reference beams to enable real-time reconstruction of the exposure position and interference pattern alignment on the camera. Data acquisition and processing were implemented using LabVIEW, which simultaneously controlled the fiber-end actuators and the XY translation stage for sequential pixelated exposure.

4.3 | Optical Characterization

The emission characteristics of the DFB lasers were measured with an inverted microscope setup (Axio Observer, Zeiss), pulsed laser and a spectrometer. The source for the pulsed laser was a frequency-tripled Nd:YAG laser (Quanta-Ray Lab-130-10, Spectra-Physics) pumping an optical parametric oscillator (OPO; versaScan, GWU Lasertechnik). As the OPO produced 5 ns pulses at a 10 Hz repetition rate, the wavelength was tuned to 490 nm according to the absorption band of the material for all measurements. This pulsed beam was coupled to the inverted microscope and focused onto the sample with an objective (20x, 0.4 NA, Zeiss). The emission signal from the sample was collected by the same objective and guided to a CMOS camera for the sample surface to be imaged. Such an image was helpful in focusing, navigating to the right pixel and choosing appropriate exposure. The emission was further guided to a spectrograph (Shamrock 303i-B, Andor) through which the laser emission spectra were acquired.

Acknowledgements

The authors gratefully acknowledge the financial support from the Innovative Doctoral Education Ecosystem for Photonics (I-DEEP, Doctoral pilot 31800022), the Photonics Research and Innovation (PREIN) Academy of Finland Flagship Programme (No. 320165), and the Centre of Excellence in Life Inspired Hybrid Materials (LIBER, No. 346147), which made this work possible. The authors also thank the Tampere Microscopy Center for access to AFM facilities, and Suvi Lehtimäki and Matias Paatelainen for their assistance with the AFM and optical characterization setups.

Open access publishing facilitated by Tampereen yliopisto ja Tampereen ammattikorkeakoulu, as part of the Wiley - FinELib agreement.

Funding

Innovative Doctoral Education Ecosystem for Photonics – I-DEEP (Doctoral pilot 31800022), Photonics Research and Innovation (PREIN), Academy of Finland Flagship Programme, No. 320165; Centre of Excellence in Life Inspired Hybrid Materials LIBER, No. 346147.

Conflicts of Interest

The authors declare no conflicts of interest.

Data Availability Statement

The data collected as part of this study can be collected from the authors upon request.

References

1. S. Chénais and S. Forget, “Recent Advances in Solid-State Organic Lasers,” *Polymer International* 61, no. 3 (2012): 390–406.
2. A. J. Kuehne and M. C. Gather, “Organic Lasers: Recent Developments on Materials, Device Geometries, and Fabrication Techniques,” *Chemical Reviews* 116, no. 21 (2016): 12823–12864.
3. I. D. W. Samuel and G. A. Turnbull, “Organic Semiconductor Lasers,” *Chemical Reviews* 107, no. 4 (2007): 1272–1295.
4. M. Sawatzki-Park, S. J. Wang, H. Kleemann, and K. Leo, “Highly Ordered Small Molecule Organic Semiconductor Thin Films Enabling Complex, High-Performance Multi-Junction Devices,” *Chemical Reviews* 123, no. 13 (2023): 8232–8250.

5. S. Riechel, U. Lemmer, J. Feldmann, et al., "Very Compact Tunable Solid-State Laser Utilizing a Thin-Film Organic Semiconductor," *Optics Letters* 26, no. 9 (2001): 593–595.
6. I. Gozhyk, M. Boudreau, H. R. Haghghi, et al., "Gain Properties of Dye-Doped Polymer Thin Films," *Physical Review B* 92, no. 21 (2015): 214202.
7. T. Dong, T. Antrack, F. Pietsch, et al., "Read My Lips: Organic Lasers on Micromachined Resonators," *Nature Communications* 16, no. 1 (2025): 7057.
8. Y. Li and G. Lakhwani, "Distributed Feedback Lasers up to the 400th Bragg Order with an Organic Active Layer," *Applied Physics Letters* 122, no. 2 (2023): 023301.
9. Y. Li and G. Lakhwani, "Active Waveguide Bragg Lasers via Conformal Contact PDMS Stamps," *Scientific Reports* 12, no. 1 (2022): 22189.
10. S. Klinkhammer, X. Liu, K. Huska, et al., "Continuously Tunable Solution-Processed Organic Semiconductor DFB Lasers Pumped by Laser Diode," *Optics Express* 20, no. 6 (2012): 6357–6364.
11. P. Görrn, M. Lehnhardt, W. Kowalsky, T. Riedl, and S. Wagner, "Elastically Tunable Self-Organized Organic Lasers," *Advanced Materials* 23, no. 7 (2011): 869.
12. C. Liu, H. Lin, D. Ji, et al., "Wavelength-Tunable Organic Semiconductor Lasers Based on Elastic Distributed Feedback Gratings," *Journal of Semiconductors* 44, no. 3 (2023): 032601.
13. L. M. Goldenberg, V. Lisinetskii, Y. Gritsai, J. Stumpe, and S. Schrader, "Single-Step Optical Fabrication of a DFB Laser Device in Fluorescent Azobenzene-Containing Materials," *Advanced Materials* 24, no. 25 (2012): 3339–3343.
14. J. R. C. Smirnov, A. Sousaraei, M. R. Osorio, et al., "Flexible Distributed Feedback Lasers Based on Nanoimprinted Cellulose Diacetate with Efficient Multiple-Wavelength Lasing," *npj Flexible Electronics* 3, no. 1 (2019): 17.
15. E. A. Prasetyanto, H. S. Wasisto, and D. Septiadi, "Cellular Lasers for Cell Imaging and Biosensing," *Acta Biomaterialia* 143 (2022): 39–51.
16. N. Toropov, G. Cabello, M. P. Serrano, R. R. Gutha, M. Rafti, and F. Vollmer, "Review of Biosensing with Whispering-Gallery Mode Lasers," *Light: Science & Applications* 10, no. 1 (2021): 42.
17. C. Kong, C. Pilger, M. Kunisch, C. Förster, J. Schulte am Esch, and T. Huser, "Hyperspectral Coherent Raman Scattering (CRS) Microscopy Based on a Rapidly Tunable and Environmentally Stable Fiber Laser," *Laser & Photonics Reviews* 17, no. 12 (2023): 2300521.
18. J. Fang, K. Huang, R. Qin, et al., "Wide-Field Mid-Infrared Hyperspectral Imaging Beyond Video Rate," *Nature Communications* 15, no. 1 (2024): 1811.
19. C. Yang, L. Liang, L. Qin, et al., "Advances in Silicon-Based, Integrated Tunable Semiconductor Lasers," *Nanophotonics* 12, no. 2 (2023): 197–217.
20. X. Liu, S. Klinkhammer, K. Sudau, et al., "Ink-Jet-Printed Organic Semiconductor Distributed Feedback Laser," *Applied Physics Express* 5, no. 7 (2012): 072101.
21. X. Liu, S. Prinz, H. Besser, et al., "Organic Semiconductor Distributed Feedback Laser Pixels for Lab-on-a-Chip Applications Fabricated by Laser-Assisted Replication," *Faraday Discussions* 174 (2014): 153–164.
22. J. A. Quintana, J. M. Villalvilla, M. Morales-Vidal, et al., "An Efficient and Color-Tunable Solution-Processed Organic Thin-Film Laser with a Polymeric Top-Layer Resonator," *Advanced Optical Materials* 5, no. 19 (2017): 1700238.
23. M. Karl, J. M. Glackin, M. Schubert, et al., "Flexible and Ultra-Lightweight Polymer Membrane Lasers," *Nature Communications* 9, no. 1 (2018): 1525.
24. Á. Farrando-Pérez, J. M. Villalvilla, J. A. Quintana, P. G. Boj, and M. A. Díaz-García, "Top-Layer Resonator Organic Distributed Feedback Laser for Label-Free Refractive Index Sensing," *Advanced Optical Materials* 12, no. 28 (2024): 2401284.
25. D. Schneider, S. Hartmann, T. Benstem, et al., "Wavelength-Tunable Organic Solid-State Distributed-Feedback Laser," *Applied Physics B* 77, no. 4 (2003): 399–402.
26. X. Liu, S. Klinkhammer, Z. Wang, et al., "Pump Spot Size Dependent Lasing Threshold in Organic Semiconductor DFB Lasers Fabricated via Nanograting Transfer," *Optics Express* 21, no. 23 (2013): 27697–27706.
27. J. Wang, T. Weimann, P. Hinze, et al., "A Continuously Tunable Organic DFB Laser," *Microelectronic Engineering* 78 (2005): 364–368.
28. P. Rochon, E. Batalla, and A. Natansohn, "Optically Induced Surface Gratings on Azoaromatic Polymer Films," *Applied Physics Letters* 66, no. 2 (1995): 136–138.
29. D. Kim, S. Tripathy, L. Li, and J. Kumar, "Laser-Induced Holographic Surface Relief Gratings on Nonlinear Optical Polymer Films," *Applied Physics Letters* 66, no. 10 (1995): 1166–1168.
30. A. Priimagi and A. Shevchenko, "Azopolymer-Based Micro- and Nanopatterning for Photonic Applications," *Journal of Polymer Science Part B: Polymer Physics* 52, no. 3 (2014): 163–182.
31. L. Rocha, V. Dumarcher, C. Denis, P. Raimond, C. Fiorini, and J. M. Nunzi, "Laser Emission in Periodically Modulated Polymer Films," *Journal of Applied Physics* 89, no. 5 (2001): 3067–3069.
32. T. Ubukata, T. Isoshima, and M. Hara, "Wavelength-Programmable Organic Distributed-Feedback Laser Based on a Photoassisted Polymer-Migration System," *Advanced Materials* 17, no. 13 (2005): 1630–1633.
33. L. M. Goldenberg, V. Lisinetskii, and S. Schrader, "Stable Lasing in Azobenzene Polyelectrolyte with Polarization Gratings as Distributed Feedback," *Advanced Optical Materials* 1, no. 10 (2013): 768–775.
34. A. Berdin, H. Rekola, O. Sakhno, M. Wegener, and A. Priimagi, "Continuously Tunable Polymer Membrane Laser," *Optics Express* 27, no. 18 (2019): 25634–25646.
35. M. Paatelainen, M. Lahikainen, A. Berdin, et al., "Hydrogel Lasers via Supramolecular Host–Guest Complexation," *Advanced Optical Materials* 11, no. 15 (2023): 2300232.
36. S. L. Oscurato, F. Reda, M. Salvatore, F. Borbone, P. Maddalena, and A. Ambrosio, "Large-Scale Multiplexed Azopolymer Gratings with Engineered Diffraction Behavior," *Advanced Materials Interfaces* 8, no. 21 (2021): 2101375.
37. S. L. Oscurato, M. Salvatore, F. Borbone, P. Maddalena, and A. Ambrosio, "Computer-Generated Holograms for Complex Surface Reliefs on Azopolymer Films," *Scientific Reports* 9, no. 1 (2019): 6775.
38. Y. Lim, B. Kang, S. J. Hong, et al., "A Field Guide to Azopolymeric Optical Fourier Surfaces and Augmented Reality," *Advanced Functional Materials* 31, no. 39 (2021): 2104105.
39. A. Berdin, H. T. Rekola, and A. Priimagi, "Complex Fourier Surfaces by Superposition of Multiple Gratings on Azobenzene Thin Films," *Advanced Optical Materials* 12, no. 4 (2024): 2301597.
40. H. Rekola, A. Berdin, C. Fedele, M. Virkki, and A. Priimagi, "Digital Holographic Microscopy for Real-Time Observation of Surface-Relief Grating Formation on Azobenzene-Containing Films," *Scientific Reports* 10, no. 1 (2020): 19642.
41. R. Kirby, R. G. Sabat, J. M. Nunzi, and O. Lebel, "Disperse and Disordered: A Mexylaminotriazine-Substituted Azobenzene Derivative with Superior Glass and Surface Relief Grating Formation," *Journal of Materials Chemistry C* 2, no. 5 (2014): 841–847.
42. M. Ristola, C. Fedele, S. Hagman, et al., "Directional Growth of Human Neuronal Axons in a Microfluidic Device with Nanotopography on Azobenzene-Based Material," *Advanced Materials Interfaces* 8, no. 11 (2021): 2100048.
43. M. Isomäki, C. Fedele, L. Kääriäinen, et al., "Light-Responsive Bilayer Cell Culture Platform for Reversible Cell Guidance," *Small Science* 2, no. 3 (2022): 2100099.
44. V. Bonal, J. A. Quintana, J. M. Villalvilla, P. G. Boj, and M. A. Díaz-García, "Controlling the Emission Properties of Solution-Processed

Organic Distributed Feedback Lasers through Resonator Design,” *Scientific Reports* 9, no. 1 (2019): 11159.

45. C. Con and B. Cui, “Effect of Mold Treatment by Solvent on PDMS Molding into Nanoholes,” *Nanoscale Research Letters* 8, no. 1 (2013): 394.

46. W. Huang, Z. Diao, Y. Liu, et al., “Distributed Feedback Polymer Laser with an External Feedback Structure Fabricated by Holographic Polymerization Technique,” *Organic Electronics* 13, no. 11 (2012): 2307–2311.

47. W. Huang, S. Shen, D. Pu, et al., “Working Characteristics of External Distributed Feedback Polymer Lasers with Varying Waveguiding Structures,” *Journal of Physics D: Applied Physics* 48, no. 49 (2015): 495105.

48. V. Bonal, R. Muñoz-Mármol, F. Gordillo Gámez, et al., “Solution-Processed Nanographene Distributed Feedback Lasers,” *Nature Communications* 10, no. 1 (2019): 3327.

49. G. A. Turnbull, P. Andrew, W. L. Barnes, and I. D. W. Samuel, “Operating Characteristics of a Semiconducting Polymer Laser Pumped by a Microchip Laser,” *Applied Physics Letters* 82, no. 3 (2003): 313–315.

50. T. Kavc, G. Langer, W. Kern, et al., “Index and Relief Gratings in Polymer Films for Organic Distributed Feedback Lasers,” *Chemistry of Materials* 14, no. 10 (2002): 4178–4185.

51. N. Viswanathan, D. Kim, S. Tripathy, et al., “Surface Relief Structures on azo Polymer Films,” *Journal of Materials Chemistry* 9, no. 9 (1999): 1941–1955.